

# Upper limit on spontaneous supercurrents in Sr<sub>2</sub>RuO<sub>4</sub>

J.R. Kirtley,<sup>1,2,3</sup> C. Kallin,<sup>4</sup> C.W. Hicks,<sup>1</sup> E.-A. Kim,<sup>5,6</sup> Y. Liu,<sup>7</sup> K.A. Moler,<sup>1,5</sup> Y. Maeno,<sup>8</sup> and K.D. Nelson,<sup>7</sup>

<sup>1</sup> Department of Applied Physics, Stanford University, Palo Alto, CA, USA

<sup>2</sup> IBM Watson Research Center, Yorktown Heights, NY, USA

<sup>3</sup> Faculty of Science and Technology and MESA<sup>+</sup> Institute for Nanotechnology, University of Twente, Enschede, The Netherlands

<sup>4</sup> Department of Physics and Astronomy, McMaster University, Hamilton, ON L8S 4M1, Canada

<sup>5</sup> Department of Physics, Stanford University, Palo Alto, CA, USA

<sup>6</sup> Stanford Institute of Theoretical Physics, Stanford University, Palo Alto, CA, USA

<sup>7</sup> Department of Physics, Pennsylvania State University, University Park, PA, 16802, USA and

<sup>8</sup> Department of Physics, Kyoto University, Kyoto 606-8502, Japan

(Dated: June 19, 2018)

It is widely believed that the perovskite Sr<sub>2</sub>RuO<sub>4</sub> is an unconventional superconductor with broken time reversal symmetry. It has been predicted that superconductors with broken time reversal symmetry should have spontaneously generated supercurrents at edges and domain walls. We have done careful imaging of the magnetic fields above Sr<sub>2</sub>RuO<sub>4</sub> single crystals using scanning Hall bar and SQUID microscopies, and see no evidence for such spontaneously generated supercurrents. We use the results from our magnetic imaging to place upper limits on the spontaneously generated supercurrents at edges and domain walls as a function of domain size. For a single domain, this upper limit is below the predicted signal by two orders of magnitude. We speculate on the causes and implications of the lack of large spontaneous supercurrents in this very interesting superconducting system.

## I. INTRODUCTION

The perovskite superconductor Sr<sub>2</sub>RuO<sub>4</sub><sup>1</sup> (T<sub>c</sub>=1.5K) is believed for a number of reasons to have unconventional pairing symmetry.<sup>2</sup> Muon spin resonance experiments are consistent with the generation of large but sparse internal magnetic fields when Sr<sub>2</sub>RuO<sub>4</sub> becomes superconducting, indicating a superconducting state with broken time reversal symmetry.<sup>3</sup> This finding is supported by the observation of the onset at the superconducting transition temperature of a Kerr effect rotation of light polarization upon reflection,<sup>4</sup> consistent with large (~50-100μm) domains with broken chiral symmetry. The first phase sensitive Josephson tunneling measurements suggested a static π-phase shift between opposite faces of a Sr<sub>2</sub>RuO<sub>4</sub> single crystal,<sup>5</sup> a result obtained only when the sample was prepared by controlled slow cooling, implying that the sample could be made to possess a small even number of domain walls separating the opposite faces. On the other hand, more recent Josephson tunneling measurements point toward small (~1μm) dynamic order parameter domains.<sup>6</sup> Magnetic imaging of the *ab* face of a single crystal of Sr<sub>2</sub>RuO<sub>4</sub> using a micron sized SQUID shows vortex coalescence on a scale of ~10 μm that may be related to a domain structure in the superconducting order parameter.<sup>7</sup> These observations, as well as others, have been interpreted in terms of a superconducting order parameter with spin triplet,<sup>8</sup> chiral  $p_x \pm ip_y$  Cooper pairing symmetry. However, Hall bar microscopy measurements<sup>9</sup> did not observe the magnetic fields expected at the surface or edges of a superconductor with broken chiral symmetry. Here, we report on new scanning SQUID microscope measurements, and we also further analyze some of the Hall bar measurements,

showing that, if they exist, the local fields at the surfaces and edges of Sr<sub>2</sub>RuO<sub>4</sub> single crystals are much smaller than those expected at the surfaces and edges of a chiral *p*-wave superconductor.

Although  $p_x \pm ip_y$  pairing symmetry is fully gapped, specific heat,<sup>10</sup> nuclear relaxation rate,<sup>11</sup> and thermal conductivity measurements<sup>12,13,14</sup> all show a power law temperature dependence, suggesting the presence of line nodes. Among other suggestions, one possibility is that the  $\gamma$  band, the band with the primary contribution to superconductivity in Sr<sub>2</sub>RuO<sub>4</sub>, has nodeless  $p_x \pm ip_y$  pairing symmetry, but induces superconductivity with a line of nodes in the other ( $\alpha$  and  $\beta$ ) bands.<sup>15</sup> Anisotropy in the gap function<sup>16</sup> has been supported experimentally by specific heat<sup>17,18</sup> and ultrasound attenuation<sup>19</sup> measurements.

The issue of the broken time reversal symmetry in the superconducting state of Sr<sub>2</sub>RuO<sub>4</sub>, aside from intrinsic interest, has taken on new urgency with several proposals for error tolerant quantum logic elements taking advantage of this property.<sup>20,21,22</sup>

There are useful analogies between a chiral  $p_x \pm ip_y$  superconductor and a ferromagnet.<sup>6,23</sup> A single domain ferromagnet has a uniform magnetization which is equivalent to the field produced by a current sheet circulating around the surface, in the appropriate geometry, while a single domain  $p_x + ip_y$  superconductor carries an intrinsic angular momentum of  $\hbar$  per Cooper pair,<sup>24</sup> which one would expect to lead to an actual surface current sheet, confined within a healing length proportional to the coherence length of the surface.<sup>25</sup> However, the field generated by this current must be screened inside the superconductor by a diamagnetic shielding current flowing within the penetration depth of the surface, so that  $B = 0$  inside the superconductor. The net result is

a spontaneous magnetization within the healing length plus the penetration depth of the sample edges, which is greatly reduced from that expected from the simple ferromagnetic analogy, but which is still substantial and, using parameters appropriate to  $\text{Sr}_2\text{RuO}_4$ , predicted to give rise to local fields as large as 1mT under certain assumptions.<sup>26,27</sup> The superconductor can also support domains in which regions of  $p_x + ip_y$  coexist with regions of  $p_x - ip_y$  order. Although the net magnetization vanishes at the boundaries between such domains, the local fields, which extend over the penetration depth on either side of the wall, can be as large as 2mT.<sup>26,27</sup> Other than direct phase sensitive measurements, the detection of such fields would be one of most direct confirmations of a superconducting order parameter with time reversal symmetry breaking since the spontaneous boundary and domain wall supercurrents are expected by symmetry<sup>28</sup> and would have no other obvious explanation. It is therefore appropriate to attempt to image the magnetic fields arising from these spontaneous supercurrents using scanning magnetic microscopy.

## II. MAGNETIC IMAGING

We have performed scanning magnetic imaging of the  $ab$  and  $ac$  faces of single crystals of  $\text{Sr}_2\text{RuO}_4$ . The magnetic images reported here were made at Stanford with a dilution refrigerator based Hall bar/SQUID microscope<sup>29</sup> with a base temperature below 100mK, and at IBM with a  $^3\text{He}$  based scanning SQUID microscope with a base temperature below 300mK. Our SQUID sensors had square pickup loops  $8\ \mu\text{m}$  on a side; the Hall bars had roughly square effective areas  $0.5\ \mu\text{m}$  on a side. The Hall bar measurements were made in a residual field of about  $2.5\ \mu\text{T}$ ; the SQUID measurements were made in a residual field of 75nT, compensated for fields perpendicular to the scanning direction to less than 10nT using a small Helmholtz coil. The SQUID measurements were made after cooling the samples through the superconducting transition temperature at a rate of about 1mK/sec. Some of the Hall bar data discussed in this paper has been reported previously.<sup>9</sup> However, here we make a more quantitative comparison of this data with theory.

The  $\text{Sr}_2\text{RuO}_4$  single crystals used in our experiments were grown using a floating zone method.<sup>30</sup> The samples used for the IBM SQUID measurements were mounted in epoxy and polished so that either the  $ab$  or  $ac$  face was part of a smooth plane, allowing scanning across the edges of the crystal.<sup>5</sup> Some of the samples used for SQUID microscopy were the same as for phase sensitive experiments on the pairing symmetry of  $\text{Sr}_2\text{RuO}_4$ ,<sup>5</sup> and had layers of SiO and  $\text{Au}_{0.5}\text{In}_{0.5}$  ( $T_c = 0.4\text{--}0.5\text{K}$ ) deposited on some of the crystal faces perpendicular to the scanned face. These additional layers should have had no effect on the magnetic imaging experiments reported here. The critical temperature of the crystals were measured to be  $> 1.4\text{K}$  using scanning and bulk susceptom-

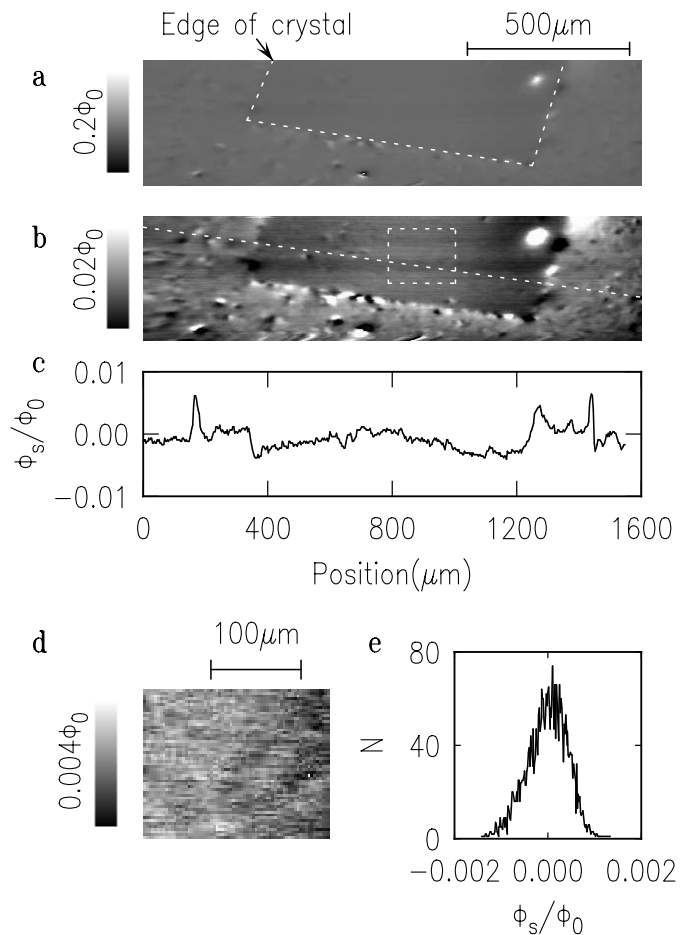


FIG. 1: SQUID microscope image of the  $ab$  face of a  $\text{Sr}_2\text{RuO}_4$  single crystal, cooled in a field  $B_z < 10\ \text{nT}$  and imaged at  $T = 0.27\text{K}$  with an  $8\ \mu\text{m}$  square pickup loop. **a** Pseudocolor image with full-scale variation of  $0.2\ \Phi_0$  ( $\Phi_0 = h/2e$ ) in magnetic flux through the SQUID pickup loop. The dashed line in **a** shows the outlines of the crystal. **b** Same image as **a**, but with the pseudocolor scale expanded to  $0.02\ \Phi_0$ . The dashed line in **b** shows the line traced by the cross-section in **c**. The dashed rectangle in **b** shows the area of the image expanded in **d**. **e** is a histogram of pixel values for the data displayed in **d**.

etry measurements.

Figure 1 shows a SQUID microscope image of the  $ab$  face of a  $\text{Sr}_2\text{RuO}_4$  single crystal. The largest feature evident in this image (Fig. 1a) is an isolated Abrikosov vortex. When the pseudocolor scale is expanded to  $\Delta\Phi_s = 0.02\Phi_0$  (Fig. 1b) magnetic features become apparent in the epoxy and along the edges of the crystal. We believe these features are not due to the superconductivity of the  $\text{Sr}_2\text{RuO}_4$  because they are unchanged from cooldown to cooldown in different fields. Figure 2 compares images from 3 different cooldowns of the same crystal, in nominal ambient plus compensating fields perpendicular to the scanning plane of zero (Fig. 2a), 10nT

(Fig. 2b), and 15nT (Fig. 2c). The number and positions of the Abrikosov vortices in the top (ab) face of the crystal, and an interlayer vortex emerging from the left (ac) face edge (Fig. 2b) of the crystal change from cooldown to cooldown, but the sharp features at the edge of the sample are remarkably reproducible. These edge features may be the result of the polishing process, such as topographical or magnetic features from particles trapped in the epoxy. Note that features very similar to the edge features are apparent in the epoxy far from the sample edge. Above the sample itself the flux image is relatively smooth, with a broad background (Fig. 1c). We believe that this broad background is the result of magnetic flux coupled into the SQUID through sections outside of the pickup loop. A clear demonstration of this effect appears in Ref. 31. On top of the broad background, two steps in the cross-section (Fig. 1c) correspond to the edges of the crystal. We believe that these steps are due to small supercurrents circulating around the entire sample due to uncompensated residual fields (see Figure 5). Figure 1d shows a magnified image of a section of the crystal (indicated by the box in Fig. 1b), with no magnetic features larger than a few  $m\Phi_0$  over an area of several hundred microns on a side.

Similar results were obtained when SQUID microscope images were taken of the *ac* face of a  $\text{Sr}_2\text{RuO}_4$  single crystal (Figure 3). In this case there were a number of interlayer vortices with flux both emerging from and entering into the crystal surface near the left edge of the crystal (Fig. 3b). Just as for the *ab* face, there were sharp magnetic features along the edges of the crystal and in the epoxy which did not appear to be correlated with the superconductivity of the  $\text{Sr}_2\text{RuO}_4$ , as well as broad magnetic backgrounds, but sharp magnetic features were absent from large areas of the crystal face.

The samples used in the Hall bar measurements were cleaved.  $1\mu\text{m}$  diameter,  $\sim 1\mu\text{m}$  deep holes were milled on a  $20\mu\text{m}$  grid on the upper surface using a focussed ion beam, to create artificial edges.<sup>9</sup> Figure 4 shows a scanning Hall bar image of the *ab* face, with a regular array of 1 micron holes at a pitch of 20 microns, of a  $\text{Sr}_2\text{RuO}_4$  single crystal. There are a few Abrikosov vortices apparent in this image, but the area away from these vortices is featureless. In particular, no features were observed in connection with the edges or interiors of the 1 micron holes. Since the  $1\mu\text{m}$  deep holes did not even act as effective pinning centers for the vortices, they may not have served as significant singularities to create edge currents. The outer edges of the crystal were not scanned in the Hall bar measurements.

### III. MODELING

Matsumoto and Sigrist<sup>26</sup> (MS) have solved the Bogoliubov-De Gennes equations using a quasi-classical approximation for the cases of an edge between a semi-infinite, ideal  $p_x + ip_y$  superconductor and vacuum, and a

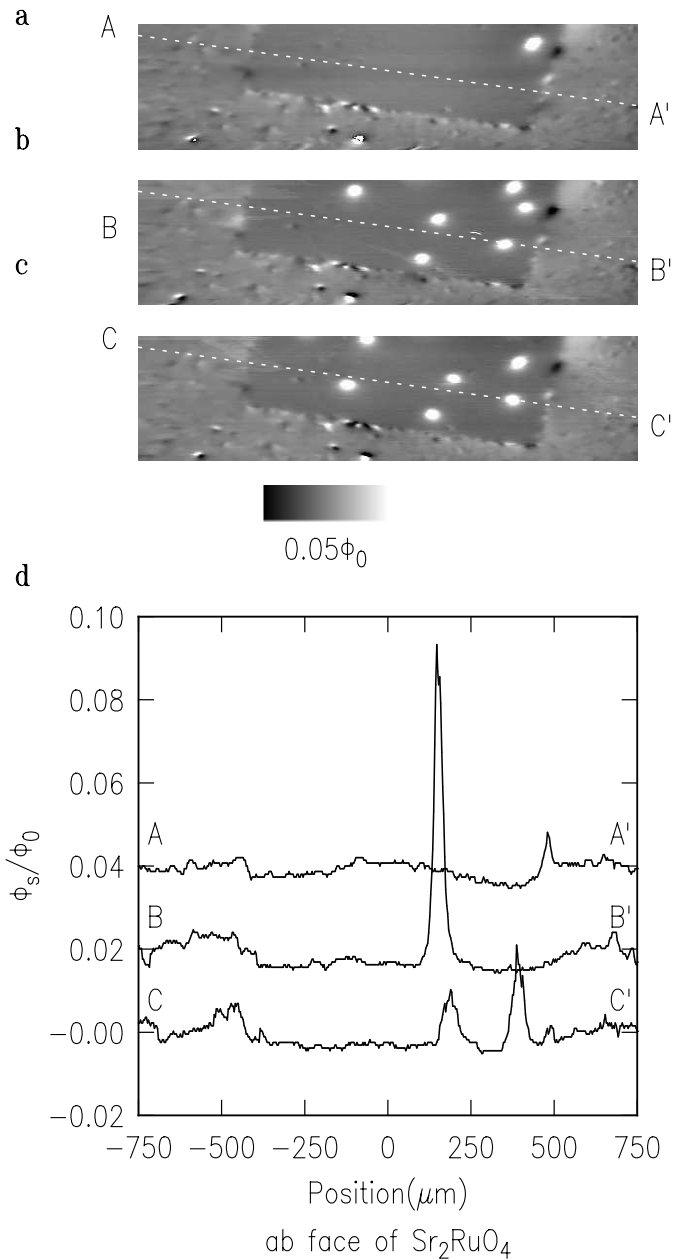


FIG. 2: Comparison of SQUID microscope images of an *ab* face of a  $\text{Sr}_2\text{RuO}_4$  crystal after three different cooldowns in slightly different magnetic fields.

domain boundary between a  $p_x + ip_y$  superconductor and a  $p_x - ip_y$  superconductor. Their solutions are fully self-consistent so that they include the effect of screening currents. They predict substantial supercurrents and consequent magnetic fields spontaneously generated at edges and domain boundaries. For example, the peak magnetic fields in these calculations correspond to 1 mT for edges, and 2 mT for domain walls using values for the coherence length ( $\xi_0=66\text{ nm}$ ) and penetration depth ( $\lambda_L=190\text{ nm}$ ) suitable for  $\text{Sr}_2\text{RuO}_4$ . However, some modeling

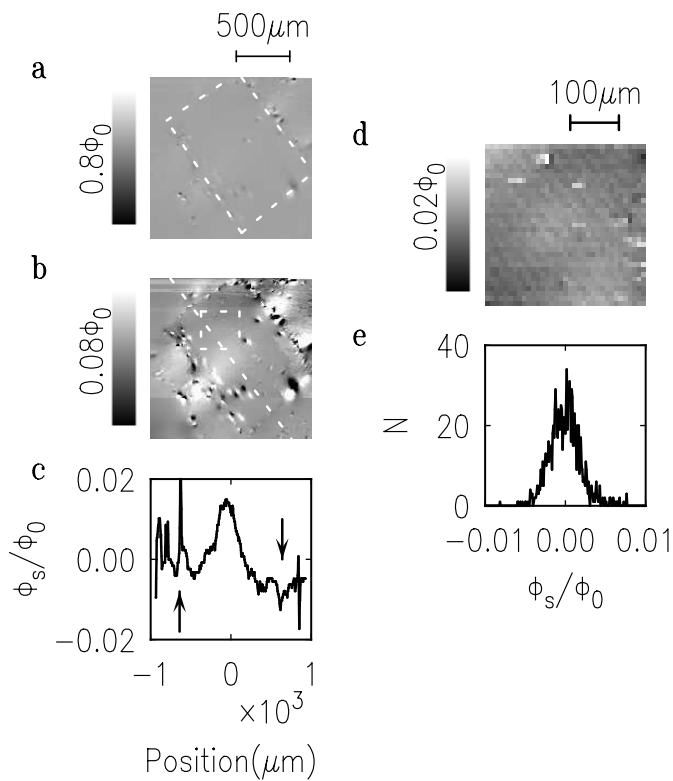


FIG. 3: SQUID microscope image of the  $ac$  face of a  $\text{Sr}_2\text{RuO}_4$  single crystal cooled in nominally zero field and imaged at  $T=0.27\text{K}$  with an  $8\ \mu\text{m}$  square pickup loop. **a** Pseudocolor image  $\Delta\Phi_s = 0.8\Phi_0$ . The dashed line in **a** shows the positions of the outer edges of the crystal. **b** Same image as **a**, but with  $\Delta\Phi_s = 0.08\Phi_0$ . A few interlayer vortices with both positive and negative signs are visible near the lower-left edge of the crystal. The dashed line in **b** is along the  $a$ -axis and shows the data traced by the cross-section in **c**. The arrows in **c** indicate the edges of the crystal. The dashed square in **b** shows the area of the image expanded in **d**. The diagonal stripes visible in **d** are due to 60 Hz noise. **e** is a histogram of pixel values for the data displayed in **d**.

is required to compare our experimental results with the MS predictions because we measure the magnetic fields above the surface, rather than inside the sample.

The simplest approach to this problem is to assume that the magnetic fields at the surface of the sample are the same as those in the bulk. This neglects field spreading and any change in superconducting shielding due to the finite sample geometry. However, in our case the size of the magnetic sensor and its spacing from the sample are large relative to the coherence length and penetration depth, so that the field averaging from these effects are larger than the additional effects of field spreading and changes in superconducting shielding. The field averaging effects from finite sensor size and height can be shown rigorously to be larger than field spreading, for example, in the similar problem of vortex fields spreading

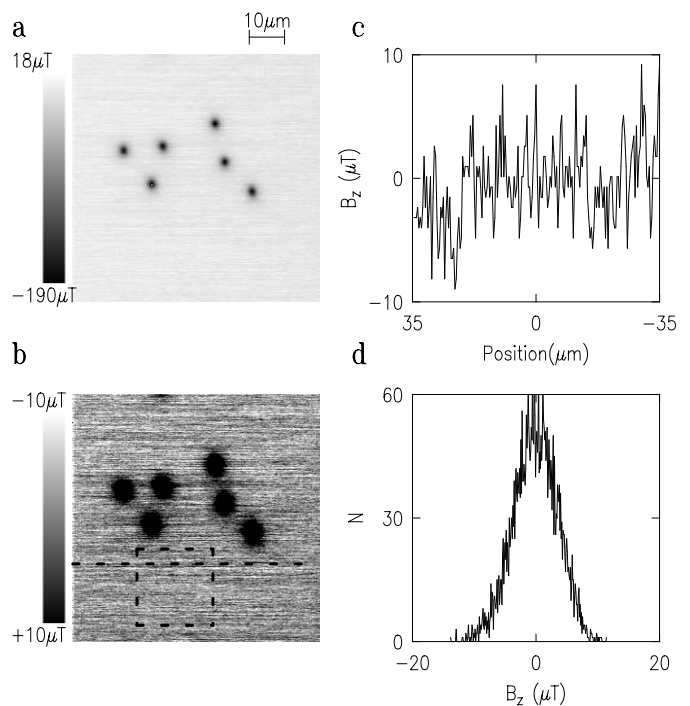


FIG. 4: **a** Scanning Hall bar image of  $ab$  face of  $\text{Sr}_2\text{RuO}_4$  single crystal, cooled in  $\sim 2.5\ \mu\text{T}$  and imaged at a temperature below  $100\text{mK}$  using a Hall bar with a sensor area  $0.5\ \mu\text{m}$  on a side. In this image the mean of each scan line was subtracted from the raw data to remove slow drift in the sensor Hall voltage. **b** Same area as **a** but with an expanded pseudocolor scale. The dashed line in **b** shows the line traced by the data cross-section in **c**. The dashed square in **b** shows the area for which a histogram of pixel inductance values are displayed in **d**.

from the surface of a superconductor and imaged with a SQUID microscope.<sup>32,33</sup> In the remainder of this section, we will neglect changes in the currents near the surface due to the finite sample geometry. We will show below that the effect of finite sample geometry only leads to suppression of the expected signal by 30% compared to what is expected from the edge currents of an infinite sample. The finite sample geometry effects for edge currents are expected to be similar to those for domain walls and are also discussed in the following section on surface screening effects.

It is well known<sup>34</sup> that if the normal component of the magnetic field  $B_z(x, y, z)$  is known at all points of a surface  $z = 0$  the magnetic field in free space at a height  $z$  above that surface is given by

$$\tilde{B}_z(k_x, k_y, z) = \tilde{B}_z(k_x, k_y, z=0)e^{-kz}, \quad (1)$$

where  $\tilde{B}_z(k_x, k_y, z)$  is the 2-dimensional Fourier transform of  $B_z(x, y, z)$  and  $k = \sqrt{k_x^2 + k_y^2}$ . To model the magnetic signals in our experimental SQUID and Hall bar microscope geometries, we assume a particular do-

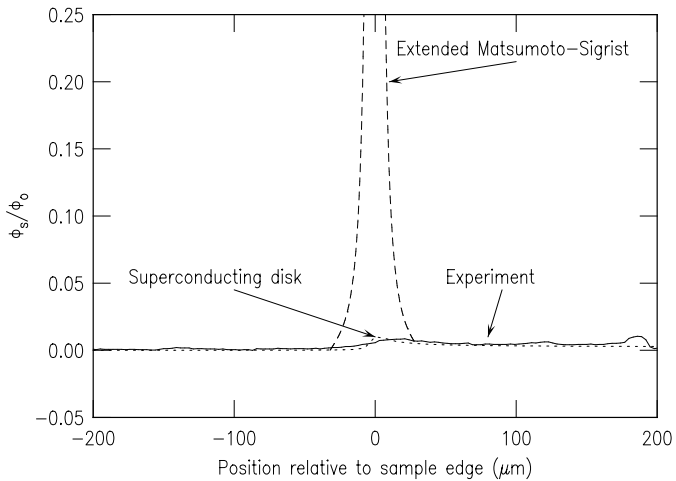


FIG. 5: Cross-section through the image of the  $ab$  face of  $\text{Sr}_2\text{CuO}_4$  displayed in Figure 1 (solid line). The short-dashed line is the prediction for a superconducting disk in a uniform residual field of 3 nT. The long-dashed line (with a peak at  $\Phi_s/\Phi_0 = 1.1$ ) is the prediction for a single domain  $p_x + ip_y$  superconductor of the extended-Matsumoto-Sigrist model as described in the text, assuming a square pickup loop  $8\mu\text{m}$  on a side, at a height of  $3\mu\text{m}$  above the sample. Here the superconductor is positioned to the left of  $0\mu\text{m}$ , with epoxy to the right.

main structure with the magnetic fields,  $B_z$ , at each edge and domain boundary, at the surface  $z = 0$ , taken to be those predicted by Matsumoto and Sigrist<sup>26</sup> for an infinite sample. We then propagate the fields to a height  $z$  using Eq. 1, integrate over an area appropriate for the SQUID or Hall bar sensor to obtain a magnetic flux, and divide by the area of the sensor for the case of the Hall bar to get an average magnetic field. We will refer to this model as the “extended-Matsumoto-Sigrist” model to distinguish it both from the prediction made by Matsumoto-Sigrist for an ideal (infinite) geometry and from the more accurate model which includes additional screening effects due to the finite geometry, as discussed in the next section. The original Matsumoto-Sigrist results are scaled in field by  $B_c = \Phi_0/2\sqrt{2}\pi\xi_0\lambda_L$ , where  $\Phi_0 = h/2e$  is the superconducting flux quantum,  $\xi_0$  is the coherence length and  $\lambda_L$  is the London penetration depth. For the modeling presented here we take  $\xi_0 = 66\text{nm}$  and  $\lambda_L = 190\text{nm}$ .<sup>2</sup>

Figure 5 compares the results of this calculation (long-dashed line) with the experimental cross-section of the image shown in Figure 1 (solid line). Also shown for comparison is the predicted cross-section for an ideal superconducting disk in a uniform residual field<sup>35</sup> of 3 nT. The small steps in flux at the edges of the crystals in Figures 1 and 3 can be attributed to shielding of a very small residual background field. These steps are much smaller than the peaks predicted by the extended-Matsumoto-Sigrist model for a single domain.

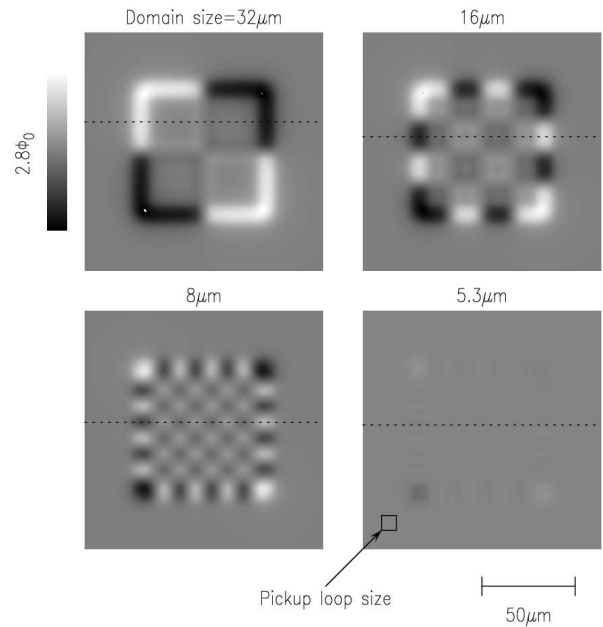


FIG. 6: Predicted magnetic fluxes through an  $8\mu\text{m}$  square pickup loop,  $3\mu\text{m}$  above the sample surface, for a  $64\mu\text{m}$  square  $p_x \pm p_y$  superconductor with various domain sizes, using the predictions for the edge and domain wall currents of Matsumoto and Sigrist as described in the text. The dashed lines in the figure show the positions of the cross-sections displayed in Fig. 7.

Figure 6 shows the results from the modeling outlined above for a series of domain sizes using parameters appropriate for our SQUID measurements. In these calculations it was assumed that the domains were square, and extended infinitely far in the negative  $z$  direction (perpendicular to the crystal face). Fig. 7 shows cross-sections through the modeling results as indicated by the dashed lines in Fig. 6. As expected, the magnetic fields above the edges and domain boundaries are averaged over a length set by both the height of the sensor above the sample surface and its size. This leads to a rapid decrease in the predicted signal when the domains become smaller than a critical length. (In this modeling the magnetic signal for a domain size of 4 microns vanishes everywhere except at the sample corners because, due to the symmetry of the domains with respect to the sensor, there

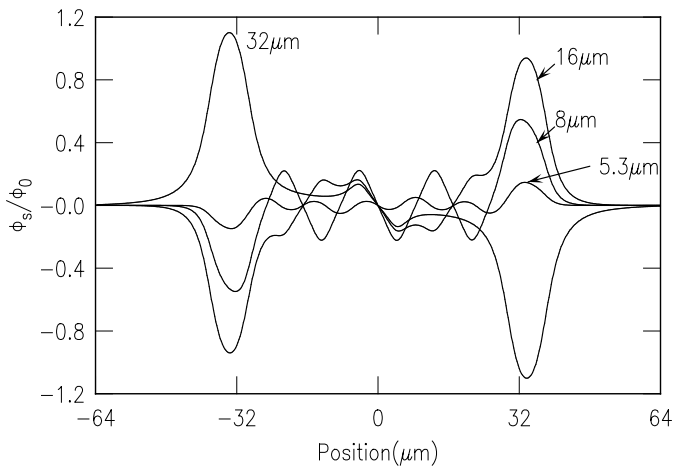


FIG. 7: Cross-sections through the modeling images of Fig. 6 for various domain sizes.

are exactly as many positive as negative contributions to the flux through the  $8\ \mu\text{m}$  diameter pickup loop. For this reason, we show the predicted flux for  $32/6=5.3$  rather than 4 micron domains.) The calculated peak values for the SQUID flux signal for edges and domain boundaries are plotted in Fig. 8a as a function of domain size. The lower dashed line in Fig. 8a is an estimate of the noise in the SQUID images above the interior of the crystals, taken to be the rms noise of the flux distribution shown in Fig. 3e ( $2.5\text{m}\Phi_0$ ). The upper dashed line is the rms value of the flux distribution above the sample edges in Fig. 1a ( $8.5\text{m}\Phi_0$ ). Comparable modeling results using parameters appropriate for our Hall bar measurements are shown in Fig. 8b. In this case the dashed line represents the rms value of the field distribution in Fig. 4d ( $3.5\ \mu\text{T}$ ). We do not display an experimental limit on the possible edge currents set by the Hall bar experiments because of uncertainties associated with the hole geometry and surface damage induced by the focussed ion beam in these experiments.<sup>9</sup>

In order to place limits on the possible field magnitude and domain sizes consistent with our results, we assume that the magnitude of the spontaneous supercurrents can vary, but that the spatial distribution of spontaneous supercurrents is as calculated by Matsumoto and Sigrist. With this assumption we can scale the results, for example, in Figs. 8a,b vertically by assuming a scaling field  $B_s$  different from  $B_c = \Phi_0/2\sqrt{2}\pi\xi_0\lambda_L$ . In order for the spontaneous supercurrents to be unobservable in our experiments, the scaling factor and domain size must be in the region below and to the left of the lines in Figs. 8c,d. Either the spontaneous currents are substantially smaller than calculated from the extended-Matsumoto-Sigrist model, or the domains are small. For example, for the SQUID measurements, the magnitude of the supercurrents at the edge must be a factor of 100 smaller than those predicted by MS if the domains are 10 or more

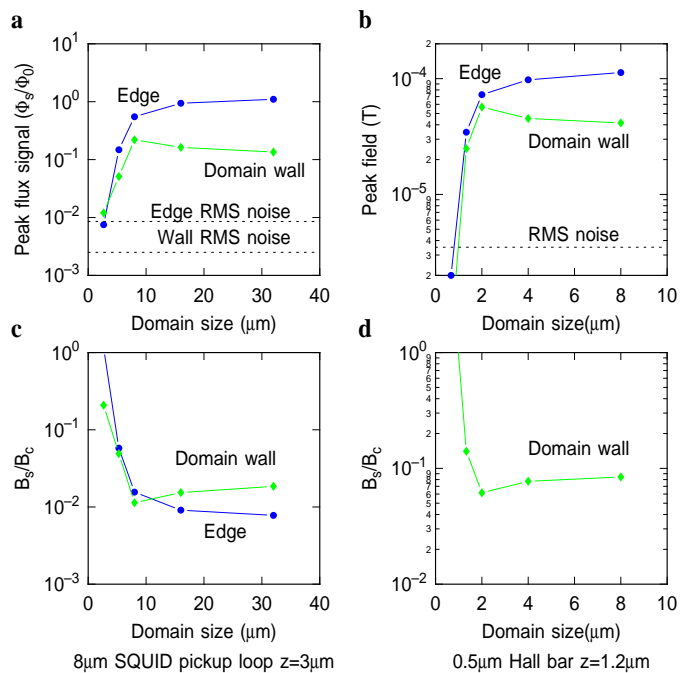


FIG. 8: **a** Plots of the predicted peak flux signals for an  $8\ \mu\text{m}$  square SQUID pickup loop,  $3\ \mu\text{m}$  above the sample surface, for a  $64\ \mu\text{m}$  square  $p_x \pm ip_y$  superconductor with various domain sizes, using the predictions of Matsumoto and Sigrist<sup>26</sup> for the spontaneously generated edge and domain supercurrents. The dashed lines represent the estimated SQUID noise in the measurements within the sample (lower line) and at the sample edges (upper line). **b** Plots of the predicted peak fields for a square Hall bar  $0.5\ \mu\text{m}$  on a side,  $1.2\ \mu\text{m}$  above the sample surface, with the corresponding Hall bar noise floor. **c** Upper limits on the size of the scaling fields  $B_s$ , normalized by  $B_c = \Phi_0/2\sqrt{2}\pi\xi_0\lambda_L$ , as a function of domain size, given by our failure to observe spontaneously generated supercurrents at edges and domain walls in the SQUID measurements. In this figure the extended-Matsumoto-Sigrist predictions are represented by  $B_s/B_c=1$ . **d** Upper limits on  $B_s/B_c$  as a function of domain size set by the Hall bar measurements.

microns in size.

#### IV. SURFACE SCREENING EFFECTS

In our modeling we have neglected the fact that the magnetic fields at the sample surface will be somewhat reduced from their bulk values. In principle, one can calculate the surface fields by self-consistently solving the Bogliubov-de Gennes equations in the appropriate geometry. Here, we simply estimate the errors involved in neglecting surface screening effects using a London approach. Following Ref. 36, the superconductor is assumed to fill the half-space  $z < 0$ . If the change in the penetration depth close to the surface is neglected, the magnetic field  $\mathbf{B}$  inside the superconductor can be de-

composed as  $\mathbf{B} = \mathbf{B}_0 + \mathbf{B}_1$ , where  $\mathbf{B}_0$  is the particular solution given by Matsumoto and Sigrist<sup>26</sup> of the inhomogeneous London's equation for a domain wall and  $\mathbf{B}_1$  is a general homogenous solution chosen to satisfy the matching conditions at  $z = 0$ . The London's equation for the particular solution can be written as<sup>36</sup>

$$k(K+k)\Phi_K = K\hat{e}_z \cdot \tilde{\mathbf{B}}_0(\mathbf{k}, 0) + i\mathbf{k} \cdot (\tilde{\mathbf{B}}_0(\mathbf{k}, 0) - 4\pi\tilde{\mathbf{M}}(\mathbf{k}, 0)), \quad (2)$$

where  $k = \sqrt{k_x^2 + k_y^2}$ ,  $K = \sqrt{k^2 + 1/\lambda^2}$ , the magnetic field  $\mathbf{B}$  above the superconductor is given by  $\mathbf{B} = -\nabla\Phi_K$ ,  $\tilde{\mathbf{B}}_0$  and  $\tilde{\mathbf{M}}$  are the 2-dimensional Fourier transforms in  $x$  and  $y$  of the inhomogeneous solution to London's equation and the volume magnetization respectively, and  $\mathbf{k} = k_x\hat{e}_x + k_y\hat{e}_y$ . However, if the domain walls are assumed to be parallel to the  $z$  axis, both  $\mathbf{B}_0$  and  $\mathbf{M}$  have only  $z$  components, and Eq. (2) reduces to

$$\Phi_K = \frac{K}{k(k+K)}\tilde{B}_{0z}(\mathbf{k}, 0), \quad (3)$$

where  $\tilde{B}_{0z}$  is the  $z$ -component of  $\tilde{\mathbf{B}}_0$ . Then

$$\tilde{\mathbf{B}}(\mathbf{k}, z) = \frac{(i\mathbf{k} + k\hat{e}_z)K}{k(k+K)}\tilde{B}_{0z}(\mathbf{k}, 0)e^{-kz}. \quad (4)$$

In our case we are only interested in the  $z$ -component of the field outside of the superconductor, which takes the particularly simple form

$$\tilde{B}_z(\mathbf{k}, z) = \frac{K}{k+K}\tilde{B}_{0z}(\mathbf{k}, 0)e^{-kz}. \quad (5)$$

The modeling in the previous section, which neglects surface shielding, is equivalent to Eq. 5 in the limit  $\lambda \rightarrow 0$ . Fig. 9 shows the effects of surface screening on the fields predicted for a single domain boundary for parameters appropriate for our Hall bar measurements. Even in this case the effects of screening are relatively small, because the penetration depth is smaller than the measuring height and size of the Hall bar. Surface screening effects would be even smaller (a few percent) for the case of SQUID imaging, because of the larger size of the sensor. The geometry for considering the effects of superconducting shielding on the edge fields is more complex than for the case of the domain boundary, as one needs to consider a superconductor bounded by both  $z$  and at least one of  $x$  or  $y$ . However, again the edge and surface effects will be confined on the scale of the penetration depth which is much smaller than the distance to the probe or the probe size. Therefore, we do not believe that the simple model presented above will be more than a factor of two different from a full calculation.

## V. DISCUSSION

If the superconductivity of  $\text{Sr}_2\text{RuO}_4$  breaks time-reversal symmetry, it should spontaneously generate supercurrents at domain boundaries and sample edges. The

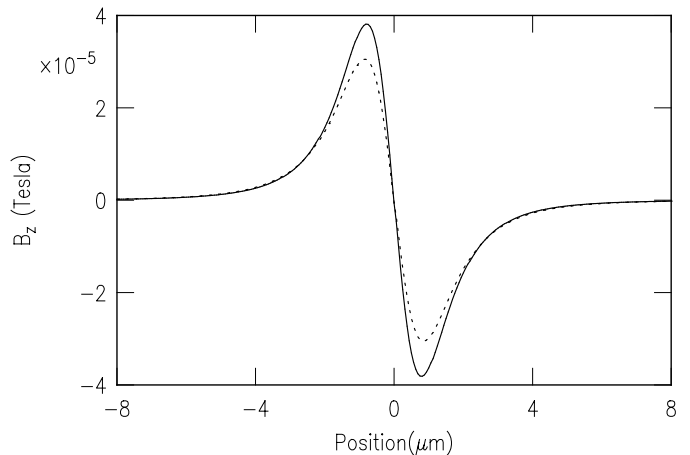


FIG. 9: Comparison of the predicted magnetic field sensed by a  $0.5 \mu\text{m}$  square Hall bar,  $1.2\mu\text{m}$  above a single domain in a  $p_x \pm ip_y$  superconductor, using the spontaneous domain currents predicted by Matsumoto and Sigrist,<sup>26</sup> with (dashed line) and without (solid line) surface screening effects as described in the text. The solid line corresponds to the extended-Matsumoto-Sigrist model.

fact that no magnetic fields due to such supercurrents were observed using scanning magnetic microscopy places significant limits on the size of these currents and the size of the domains, as shown in Fig. 8. In particular, from the combined Hall bar and SQUID measurements, we conclude that if the spontaneous supercurrents at a domain wall are of the size expected from the calculations of Matsumoto and Sigrist<sup>26</sup> and the modelling done here, one can set a conservative upper limit on the domain size of 1.5 microns for both interior and edge domains. Alternatively, if the domains intersecting the  $ab$  face are 10 microns or more in size, we conclude that the spontaneous supercurrents at edges are a factor of 100 smaller than expected from the calculations of Matsumoto and Sigrist combined with our modelling.

Calculations of the self-consistent screening currents employed in our modelling have assumed an ideal  $p_x \pm ip_y$  superconducting gap symmetry.<sup>26</sup> However, for  $\text{Sr}_2\text{RuO}_4$ , the gap in the  $ab$  plane is believed to be anisotropic.<sup>17,18</sup> In addition, three different bands contribute to the Fermi surface in  $\text{Sr}_2\text{RuO}_4$ .<sup>2</sup> These properties are likely to impact on the magnitude of the self-consistent screening currents, although, a priori, it is not clear whether the magnitude would be increased or decreased from the values calculated by MS. On the other hand, muon spin resonance observed internal fields which are roughly consistent with the predicted values.<sup>3</sup> If these observed fields are due to internal domain walls, it suggests that the surface currents must be reduced by two or more orders of magnitude from their bulk values if the domains are larger than 10 microns. It is difficult to imagine what could so strongly reduce the surface fields at the  $ab$  sur-

face due to domain boundaries. The surface screening effects are small; the surfaces are cleaved; and roughness even to the depth of a hundred angstroms or so will not substantially reduce the fields detected at the Hall probe or SQUID. This suggests that domains intersecting the ab plane are either so sparse as to not have been scanned or are smaller than a few microns. Another possibility is that the domains intersecting the ab surface are shallow, with a depth along the c-axis noticeably less than the penetration depth. In this case, the spontaneous currents and fields could be too weak and spread out in the ab layers to be detected. However, we note that either small domains or domains shallower than the optical skin depth would also interfere with observations of the Kerr effect rotation.

Sufficient roughness of the ac or bc faces can be expected to have a more noticeable effect on the edge or boundary currents. The samples used for the SQUID measurements on these faces were polished and AFM imaging on typical samples show them to be smooth to 5 nm (rms).<sup>37</sup> MS assumed specular scattering from the edge in which case one component of the order parameter is suppressed while the other component is slightly enhanced. For diffuse scattering from a rough edge, both components will be suppressed and this will reduce the surface currents and resulting magnetic fields. Although self-consistent calculations have not been carried out for this case, the effect of surface roughness on the two component order parameter has been studied,<sup>38</sup> and one finds that the two components heal over quite different length scales. Using Ginzburg-Landau and London theory to estimate the resulting change in the surface magnetization, one finds that, even for completely diffuse scattering from a rough surface, the reduction in surface magnetization is less than 30%.<sup>39</sup>

Domain walls cost energy because they disrupt the superconducting order. Unlike a ferromagnet, there is no balancing of this energy due to dipolar forces because spontaneous screening currents ensure that the magnetic field, or local magnetization, is zero inside the superconductor. Therefore, in principle, a single domain  $p_x + ip_y$  superconductor is possible. However, domains will naturally form as the sample is cooled through  $T_c$  and as extended objects, these domains are susceptible to pinning by defects and impurities in the sample. Therefore, one expects domains to be present although their density may be controlled by sample purity and slow cooling in a field. Muon spin resonance experiments were interpreted as evidence for dilute domains,<sup>3</sup> Kerr effect measurements suggested domain sizes in the range of 50 to 100 microns,<sup>4</sup> while the first phase sensitive Josephson tunneling measurements are consistent with no domains (or a small even number of domain walls between opposing faces of the crystal).<sup>5</sup> On the other hand, more recent Josephson tunneling measurements were interpreted as evidence for dynamic domains of  $\sim 1$  micron on average,<sup>6</sup> although one would extract larger domain sizes if finite domains perpendicular to the c-axis were included in the

modelling. All of these measurements, except for muon spin resonance, would see reduced signals if the domain size along the c-axis becomes small and this would affect the measurements reported here as well. Unless the fields at domain walls are reduced by more than an order of magnitude in size from the predicted values, the Hall bar measurements suggest domain sizes of either less than 1.5 microns in size over the ab face or large enough that no domain wall fell in the  $100 \times 100 \mu\text{m}$  scan area.

Earlier work has reported that large domains can be flipped by fields of the order of a mT or larger<sup>4</sup> and that small surface domains are influenced by fields  $< 0.1 \mu\text{T}$ .<sup>6</sup> While the data presented here was taken on samples cooled in fields less than  $2.5 \mu\text{T}$ , Hall data taken on samples cooled in up to a mT was very similar to that shown here except for the presence of more trapped vortices.<sup>9</sup> In principle, very fast domain wall motion could result in zero time-averaged edge current and zero time-averaged domain wall current. However, previous experiments<sup>4,5,6</sup> suggest that the domain wall motion would be slow on our experimental time scale, which is 10 seconds per line scan for the scanning SQUID microscope data shown here. Therefore, it is unlikely that dynamic behavior of the domains prevents the observation of the signal in this experiment.

In conclusion, scanning magnetic microscopy measurements place quite severe limits on the size of edge currents and/or on domain sizes in  $\text{Sr}_2\text{RuO}_4$ . The different experimental results taken as evidence for  $p_x + ip_y$  pairing come to quite different conclusions about domain sizes. Since there are now detailed predictions for the field profile in the vicinity of domain walls in the bulk, muon spin resonance could now, in principle, provide detailed information about the validity of these predictions as well as quantitative information about the density of domains in the bulk. In addition, either slow muons<sup>40</sup> or beta-NMR<sup>41</sup> could be used to probe the surface region and to look for fields due to spontaneous edge currents as well as domains near the surface. Scanning magnetic microscopy is still one of the most direct probes of domains intersecting the surface and of edge currents and further improvements in sensitivity may either confirm or rule out their existence.

## VI. ACKNOWLEDGEMENTS

We would like to thank H. Bluhm, J. Berlinsky, S.B. Chung, M. Franz, H. Hilgenkamp, T.-L. Ho, M. Matsumoto, M. Sigrist and M. Stone for many useful discussions and H. Bluhm for also sharing the results of his calculations before publication. We would also like to thank P. Björnsson for sharing his Hall bar data with us. This work was supported by DOE at Stanford under grant DE-AC02-76SF00515. Work at Penn State was supported by DOE under grant DE-FG02-04ER46159. JRK was supported by the Center for Probing the Nanoscale, an NSF NSEC, NSF Grant No. PHY-0425897, and by the

Dutch NWO Foundation. In addition, CK acknowledges the hospitality of the Stanford Institute for Theoretical Physics and the Kavli Institute for Theoretical Physics

during this collaboration and the support of the National Science Foundation under Grant No. PHY05-51164.

- 
- <sup>1</sup> Y. Maeno, H. Hashimoto, K. Yoshida, S. Nishizaki, T. Fujita, J.G. Bednorz and F. Lichtenberg, *Nature* **372** 532 (1994).
- <sup>2</sup> A.P. Mackenzie and Y. Maeno, *Rev. Mod. Phys.* **75**, 657 (2003).
- <sup>3</sup> G.M. Luke et al., *Nature* **394**, 558 (1998).
- <sup>4</sup> J. Xia, Y. Maeno, P.T. Beyersdorf, M.M. Fejer, and A. Kapitulnik, *Phys. Rev. Lett.* **97**, 167002 (2006).
- <sup>5</sup> K.D. Nelson, Z. Q. Mao, Y. Maeno, and Y. Liu, *Science* **306**, 1151 (2004).
- <sup>6</sup> F. Kidwingira, J.D. Strand, D.J. van Harlingen, Y. Maeno, *Science* **314**, 1267 (2006).
- <sup>7</sup> V.O. Dolocan, C. Veauvy, F. Servant, P. Lejay, K. Hasselbach, Y. Liu, and D. Mailly, *Phys. Rev. Lett.* **95**, 097004 (2005).
- <sup>8</sup> The evidence for spin-triplet pairing comes from NMR-Knight shift experiments. See K. Ishida, H. Mukuda, Y. Kitaoka, K. Asayama, Z. Q. Mao, Y. Mori, and Y. Maeno, *Nature* **396**, 658 (1998); H. Murakawa, K. Ishida, K. Kitagawa, Z. Q. Mao, and Y. Maeno, *Phys. Rev. Lett.* **93**, 167004 (2004).
- <sup>9</sup> P.G. Björnsson, Y. Maeno, M.E. Huber, and K.A. Moler, *Phys. Rev. B* **72**, 012504 (2005).
- <sup>10</sup> S. NishiZaki, Y. Maeno, and Z. Mao, *J. Phys. Soc. Jpn.* **69**, 572 (2000).
- <sup>11</sup> K. Ishida, H. Mukuda, Y. Kitaoka, Z.Q. Mao, Y. Mori, and Y. Maeno, *Phys. Rev. Lett.* **84**, 5387 (2000).
- <sup>12</sup> M.A. Tanatar, S. Nagai, Z.Q. Mao, Y. Maeno, and T. Ishiguro, *Phys. Rev. B* **63**, 064505 (2001).
- <sup>13</sup> M.A. Tanatar, M. Suzuki, S. Nagai, Z.Q. Mao, Y. Maeno, and T. Ishiguro, *Phys. Rev. Lett.* **86**, 2649 (2001).
- <sup>14</sup> K. Izawa et al., *Phys. Rev. Lett.* **86**, 2653 (2001).
- <sup>15</sup> M.E. Zhitomirsky and T.M. Rice, *Phys. Rev. Lett.* **87**, 057001 (2001).
- <sup>16</sup> K. Miyake and O. Narikiyo, *Phys. Rev. Lett.* **83**, 1423 (1999).
- <sup>17</sup> K. Deguchi, Z.Q. Mao, H. Yaguchi, and Y. Maeno, *Phys. Rev. Lett.* **92**, 047002 (2004).
- <sup>18</sup> K. Deguchi, Z.Q. Mao, and Y. Maeno, *J. Phys. Soc. Jpn.* **73**, 1313 (2004).
- <sup>19</sup> C. Lupien, W.A. MacFarlane, C. Proust, L. Taillefer, Z.Q. Mao, and Y. Maeno, *Phys. Rev. Lett.* **86**, 5986 (2001).
- <sup>20</sup> A.M. Zagoskin, G. Rose, M.H.S. Amin, M. Franz, and J.P. Hilton, U.S. Patent 6504172.
- <sup>21</sup> A.M. Zagoskin, J.P. Hilton, M.H.S. Amin, G. Rose, and M. Franz, U.S. Patent 6537847.
- <sup>22</sup> S. Das Sarma, C. Nayak, and S. Tewari, *Phys. Rev. B* **73**, 220502(R) (2006).
- <sup>23</sup> T.M. Rice, *Science* **314**, 1248 (2006).
- <sup>24</sup> T. Kita, *J. Phys. Soc. Japan* **67**, 216 (1998).
- <sup>25</sup> M. Stone and R. Roy, *Phys. Rev. B* **69**, 184511 (2004).
- <sup>26</sup> M. Matsumoto and M. Sigrist, *J. Phys. Soc. Jpn.* **68**, 994 (1999); erratum op cit. p. 3120; cond-mat/9902265.
- <sup>27</sup> H-J Kwon, V.M. Yakovenko and K. Sengupta, *Synth. Metals* **133-134**, 27 (2003).
- <sup>28</sup> M. Sigrist and K. Ueda, *Rev. Mod. Phys.* **63**, 239 (1991).
- <sup>29</sup> P.G. Björnsson, B.W. Gardner, J.R. Kirtley, and K.A. Moler, *Rev. Sci. Instrum.* **74**, 4153 (2001).
- <sup>30</sup> Z. Q. Mao, Y. Maeno, and H. Fukazawa, *Mater. Res. Bull.* **35**, 1813 (2000).
- <sup>31</sup> J.R. Kirtley, A.C. Mota, M. Sigrist, and T.M. Rice, *J. Phys.: Condens. Matter* **10**, L97 (1998).
- <sup>32</sup> A.M. Chang, H.D. Hallen, L. Harriott, H.F. Hess, H.L. Kao, J. Kwo, R.E. Miller, R. Wolfe, and J. van der Ziel, *Appl. Phys. Lett.* **61**, 1974 (1992).
- <sup>33</sup> J. R. Kirtley, V. G. Kogan, J. R. Clem, and K. A. Moler, *Phys. Rev. B* **59**, 4343 (1999).
- <sup>34</sup> B.J. Roth, N.G. Sepulveda, and J.P. Wikswo, *J. Appl. Phys.* **65**, 361 (1988).
- <sup>35</sup> J.D. Jackson, "Classical Electrodynamics, Third Edition", New York, Academic Press, 1999, p. 129.
- <sup>36</sup> H. Bluhm, preprint.
- <sup>37</sup> K.D. Nelson, Ph.D. thesis, <http://etda.libraries.psu.edu/theses/approved/WorldWideIndex/ETC-726/index.html>.
- <sup>38</sup> Y. Nagato, M. Yamamoto and K. Nagai, *J. Low. Temp. Phys.* **110**, 1135 (1998).
- <sup>39</sup> C. Kallin, unpublished.
- <sup>40</sup> M. Sigrist, private communication.
- <sup>41</sup> Z. Salman, R.F. Kiehl, K.H. Chow, W.A. MacFarlane, S.R. Kreitzman, D.J. Arseneau, S. Daviel, C.D.P. Levy, Y. Maeno, and R. Poutissou, *Physica B* **374-375** 468 (2006).